Real-Time Digital PWM With Zero Baseband Distortion and Low Switching Frequency

Fernando Chierchie, *Graduate Student Member, IEEE*, and Eduardo E. Paolini

***Abstract*—A discrete-time pulse width modulator (PWM) with zero baseband distortion for arbitrary band-limited modulating signals is developed in this paper. It is based on adjusting the duty-cycles of the PWM such that the samples of an ideal low-pass filtered version of the PWM signal coincide with the discrete-time samples of the modulating signal. Elaborating on previous approaches in the literature, it is shown that this problem can be stated as a multidimensional inverse function approach, and therefore it can be solved using iterative methods. Starting with the duty-cycle values of a uniform PWM, the successive iterations provide slight duty-cycle corrections that, in the limit, result in zero baseband distortion even for low carrier-to-modulating frequency ratios. Aiming at a practical, real-time implementation two new results are provided. First, explicit bounds on the improvement achievable after each duty-cycle correction are derived. Second, a block processing architecture suitable for real-time implementation is proposed, and the increase of distortion caused by its use is quantified. Several examples with typical band-limited signals demonstrate the performance of the algorithm.**

***Index Terms*—Digital modulation, harmonic distortion, power amplifier, pulse width modulation, switching amplifier.**

I. Introduction

EFFICIENT power amplification has attracted the attention of the researches since the pioneering efforts of Black [1], with his formalization of several pulse-modulation techniques. One of the preferred techniques is pulse-width modulation (PWM), with its almost endless variations and alternatives.

The traditional, "analog" PWM, known as natural PWM (NPWM), has reduced harmonic content within the baseband. This distortion is composed of the sidebands of the carrier frequency, and for practical applications it can be reduced to negligible levels by increasing the carrier frequency. Its discrete-time implementation, known as uniform PWM (UPWM), exhibits far greater harmonic distortion, composed not only of the sidebands of the carrier frequency, but also of the derivatives of the modulating signal [2]–[6], and therefore it cannot be reduced by the same amount by increasing the carrier frequency. In any case, this in-band distortion cannot be removed by the traditional low-pass filter that acts as a demodulator in almost every PWM scheme.

Recent research efforts are devoted to develop variants to the PWM modulation scheme to reduce or to eliminate the distortion within certain frequency band, usually the baseband. Some of these approaches are designed to attenuate certain specific harmonics [7], or to emulate the behavior of NPWM (pseudo natural PWM) [8]–[10], reducing or eliminating the harmonics of the modulating signal. These schemes are usually based on the assumption that the switching frequency is much greater than the maximum frequency of the modulating signal.

A different alternative is to devise a modulation algorithm that produces no distortion components within the baseband. This approach is of interest, for example, in the neuroscience field [11], [12], where algorithms for time encoding/decoding of band-limited signals with perfect recovery have been developed; however, the demodulation process is not practical for power applications. One of the first attempts to address this problem was click modulation [13], [14]. Based on the properties of analytic signals, this complex modulation scheme is capable of representing band-limited signals using PWM-like waveforms with zero distortion in the baseband. It has not received much attention for several years, but recently this method has captured the consideration of the researchers [14], [15]. Although it is not well-suited for online implementation, new developments could change this scenario [16]. In this direction, recent results have shown that band-limited, bounded signals can be represented using two or three level PWM signals with no distortion in the baseband using low frequency carriers. In [17], the problem of determining the duration and position of the pulses to minimize the average switching frequency with in-band error-free encoding has been addressed. The solution requires to equate certain number of coefficients of the Fourier series of the modulating and of the PWM signal, and solving a nonlinear system of simultaneous equations. The result is a variable-frequency PWM signal, where the average switching frequency can be slightly higher than the maximum harmonic component of the modulating signal. Although some considerations are provided for the modulation of non-periodic signals, the method is not well suited for on-line implementation, not only because the result is signal dependent, but also because the knowledge of the entire modulating signal is required. Another approach is studied in [18], where the modulation problem is stated as determining the duty-cycles of a fixed frequency PWM signal such that the samples of an ideal low-pass filtered version of the PWM signal coincide with the samples of the modulating signal, converting variable amplitude discrete-time samples to fixed amplitude, variable width pulses. The solution also requires to solve a nonlinear system of simultaneous equations, and an ad-hoc iterative algorithm is provided that guarantees

Manuscript received September 10, 2012; revised December 21, 2012; accepted February 05, 2013. Date of publication June 03, 2013; date of current version September 25, 2013. This work was supported in part by CONICET, CIC and SGCyT-UNS (PGI 24ZK21 and PGI 24K055). This paper was recommended by Associate Editor M. Laddomada.

The authors are with the Instituto de Investigaciones en Ing. Electrica (IIIE) Alfredo Desages (UNS-CONICET) and the Dto. de Ing. Electrica y de Computadoras, Universidad Nacional del Sur, 8000 Bahia Blanca Argentina. (e-mail: fernando.chierchie@uns.edu.ar; epaolini@uns.edu.ar).

Color versions of one or more of the figures in this paper are available online at http://ieeexplore.ieee.org.

Digital Object Identifier 10.1109/TCSI.2013.2249171

exponential convergence. In [19] the relationship between the modulating signal samples and the pulse widths is modeled with a Volterra filter, and its inverse is used as a prefilter to reduce the nonlinear distortion.

In this paper we develop a PWM coding algorithm for discrete-time signals that exhibits no distortion in the baseband, and propose an architecture that is suitable for real-time operation. These characteristics are preserved even for low PWM carrier frequencies. The method is based on solving the same problem as that in [18], i.e., determining the duty-cycles of the PWM signal such that the samples of an ideal low-pass filtered version of the PWM signal coincide with the discrete-time samples of the modulating signal. Our developments extend their results by making the following contributions: 1) demonstration that this approach can be recast into the solution of a multidimensional inverse function problem that can be solved using standard iterative methods, 2) quantification of the distortion level that is achievable after adjusting the duty-cycles in each iteration, and 3) development of a structure suitable for real-time implementation based on overlapped block processing, and the derivation of performance measures that quantify the increase of the distortion caused by the finite length of the blocks.

The performance of the algorithm is demonstrated using several test signals: low and high (near Nyquist) frequency sinusoids, sum of sinusoids for standard intermodulation distortion (IMD) evaluation, filtered random noise, and a fragment of a musical score. It is shown that very low distortion levels, with an in-band signal to noise ratio (SNR) exceeding 90 dB can be achieved, even when using a low frequency carrier. This results in reduced switching losses, which are of paramount importance for portable and/or high power applications. If the PWM carrier frequency is increased, SNR can be further enhanced, allowing the designer to trade-off between high efficiency amplification or simpler reconstruction filter.

The paper is organized as follows. Section II summarizes the spectral characteristics of PWM signals. The problem of computing the duty-cycles that yield in-band error-free PWM using an inverse function approach is studied in Section III. In Section IV a block processing architecture suitable for real-time implementation is developed together with explicit expressions that quantify its impact on the baseband distortion level. The computational complexity of the algorithm is also discussed, and several alternatives to reduce the computational load are explored, resulting in an algorithm that is suitable to run in standard hardware. Finally, simulation results for several band-limited signals are given in Section V, and some concluding remarks are given in Section VI.

II. Brief Review of the Spectrum of PWM Signals

A three level PWM signal can be represented mathematically as [2], [18]

$$p(t) = \sum_{n=-\infty}^{\infty} \left[u\left(t - nT + w_n \tfrac{T}{2}\right) - u\left(t - nT - w_n \tfrac{T}{2}\right) \right] \tag{1}$$

where $u(t)$ is the unit-step function, T is the PWM period, and w_n is the normalized duty-cycle of the n-th pulse, with $w_n \in (-1,\ 1)$[1].

[1]A two-level PWM signal $p_2(t)$ can also be represented by limiting the normalized duty-cycle to $w_n \in (0,\ 1)$, and defining $p_2(t) = 2p(t) - 1$.

Given a band-limited modulating signal $x(t)$ with a maximum frequency of f_m, a discrete-time PWM modulator can be thought as a device that maps the samples $x_n = x(t)|_{t=nT}$ into a set of normalized duty-cycles w_n, $n \in \mathbb{Z}$. Without loss of generality, and to simplify the presentation, it will be assumed that the sampling frequency is $f_s = 1/T$ coinciding with the PWM frequency.

One of the most common discrete-time PWM modulators is known as Symmetrical Double Edge Uniform PWM (SDEUPWM). The PWM signal is obtained by comparing the samples x_n of the modulating signal with the output of an ascending/descending counter. The frequency spectrum of SDEUPWM for an arbitrary band-limited modulating signal $x(t)$ is given by [2],

$$P(f) = e^{-j\pi fT}\left[X(f) + X_1(f) + X_2(f)\right], \tag{2}$$

where $X(f)$ is the Fourier transform of $x(t)$ and

$$X_1(f) = \sum_{n=1}^{\infty} \frac{(j\pi fT)^{2n}}{2^{2n}(2n+1)!} W_{2n+1}(f),$$

$$X_2(f) = \sum_{k=1}^{\infty}\sum_{n=1}^{\infty} \frac{(j\pi fT)^{2n+1}}{2^{2n}} \left[W_{2n+1}(f + kf_s) + W_{2n+1}(f - kf_s)\right]$$

with $W_n(f)$ being the Fourier transform of $[1 + x(t)]^n$. The transform $X_1(f)$ represents the baseband distortion component of the modulation, and $X_2(f)$ represents the lateral side-bands of the carrier frequency and its multiples. These harmonics are weighed by a factor $1/2^{2n}$, and, therefore, their baseband effect is negligible if $f_s/f_m \gg 1$, which is typical in practical applications. Under this assumption, the PWM signal in the baseband can be approximated by

$$y(t) \approx x\left(t - \tfrac{T}{2}\right) + \frac{T}{32}\frac{d^2}{dt^2}\left[x\left(t - \tfrac{T}{2}\right) + x^2\left(t - \tfrac{T}{2}\right)\right], \tag{3}$$

mainly including contributions from $X(f)$ and $X_1(f)$. For low f_s/f_m ratios, the distortion is increased not only because of the derivatives in (3), but also because of the side-bands due to $X_2(f)$ in (2).

III. PWM With Zero Baseband Distortion

In [18] it is shown that every band limited signal $x(t)$ of bandwidth f_m, bounded to $|x(t)| < 2/\pi$ can be represented by a PWM signal with fixed carrier frequency $f_s \geq 2f_m$, and that $x(t)$ can be recovered with zero baseband distortion through ideal low pass filtering. The $2/\pi$ constraint is a theoretical limit that must be satisfied to ensure that any band-limited signal can be represented as a PWM waveform with zero baseband distortion. This bound depends directly on the ratio between the PWM frequency and the maximum frequency of the modulating signal, and its lowest bound $2/\pi$ is attained when the PWM frequency equals the Nyquist frequency $f_s = 2f_m$. Although this restriction may seem severe, it can be easily circumvented in practical applications. Violation of this bound results in a reduced (non-zero) distortion content within the baseband, that still is far lower than that achieved with typical PWM implementations as it is shown in Section V-C.

In the following, we show that the problem of determining the normalized duty-cycles of the PWM signal such that the sample values of the ideally low pass filtered PWM signal coincides with the samples of the modulating signal can be recast into

an inverse function problem. The advantage of adopting this framework is that several results regarding iterative solutions, rates of convergence and error bounds can be used to quantify the distortion level achieved in this application.

The PWM signal $p(t)$ in (1) is composed of a pulse train of widths w_n, $-\infty < n < \infty$, that are a function of the samples of the modulating signal x_n, typically a scaled version. Filtering the PWM signal $p(t)$ with a ideal low-pass filter results in the continuous-time signal $y(t) = h_{LP}(t) * p(t)$, where "$*$" stands for the continuous convolution operation and $h_{LP}(t) = f_s \operatorname{sinc}(f_s t)$ is the impulse response of the ideal low-pass filter with the cut-off frequency $f_s/2$ and unity gain. Uniform sampling of $y(t)$ at a rate $T = 1/f_s$ results in the demodulated signal sample y_n, whose value at the n-th sample is given by [18], [19]

$$\begin{aligned} y_n &= \sum_{k=-\infty}^{\infty} f_k(w_{n-k}) \\ &= f_0(w_n) + \sum_{k=1}^{\infty} [f_k(w_{n-k}) + f_k(w_{n+k})] \end{aligned} \tag{4}$$

with

$$f_k(w) \triangleq \frac{\left(\operatorname{Si}\left[k\pi + w(\frac{\pi}{2})\right] - \operatorname{Si}\left[k\pi - w(\frac{\pi}{2})\right]\right)}{\pi} \tag{5}$$

where $\operatorname{Si}(z) = \int_0^z \sin(\tau)/\tau d\tau$ is the sine-integral function. Equation (4) takes advantage of the even symmetry of $f_k(w)$ with respect to k, i.e., $f_k(w) = f_{(-k)}(w)$. The first term describes the contribution of the n-th duty-cycle to the value of the n-th demodulated signal sample, while the second represents the contribution of the remaining pulses.

Let $\mathbf{x}$, $\mathbf{y}$, $\mathbf{w}$ be the N-dimensional vectors composed of N samples of the modulating signal $x(t)$, the filtered PWM signal $y(t)$ and the duty-cycles w_n, $n = 0, \ldots, N-1$, respectively. Then, (4) can be rearranged as

$$y_n = f_0(w_n) + \sum_{k=1}^{N-1-n} f_k(w_{n+k}) + \sum_{k=1}^{n} f_k(w_{n-k}) \tag{6}$$

and therefore

$$\mathbf{y} = \mathbf{g}(\mathbf{w})$$

where the mapping $\mathbf{g} : \mathbb{R}^N \to \mathbb{R}^N$ relates the vector of duty-cycles $\mathbf{w} \in \mathbb{R}^N$ to the samples of the filtered PWM signal $\mathbf{y} \in \mathbb{R}^N$.

Under this setting, the determination of the vector of duty-cycles $\mathbf{w}$ to achieve zero distortion within the baseband can be stated as follows:

Problem Statement: Given the vector $\mathbf{x}$ of modulating signal samples, find the vector $\mathbf{w}^*$ of duty-cycles such that $\mathbf{g}(\mathbf{w}^*) - \mathbf{x} = 0$. If $\mathbf{w}^*$ exists then the PWM signal $p(t)$ has zero distortion in the band $[0,\ f_s/2)$.

The solution of the modulation problem is given by $\mathbf{w}^* = \mathbf{g}^{-1}(\mathbf{x})$, but explicit inversion is generally not possible for large values of N. A numerical, iterative procedure to compute $\mathbf{w}^*$ is proposed next.

A. Numerical Solution

The zeros $\mathbf{w} = \mathbf{w}^*$ of $\mathbf{g}(\mathbf{w}) - \mathbf{x} = \mathbf{0}$ can be computed iteratively using Newton-Raphson techniques. The convergence of the recursion is ensured by Theorem 1 below. To account for worst case error analysis the infinity norm for vectors, $\|\mathbf{x}\|_\infty \triangleq \max_{1\le i\le N}(|x_i|)$, and the correspondent induced matrix norm $\|\mathbf{X}\|_{\infty_i} \triangleq \max_{1\le j\le N}(\sum_{i=1}^{N} |x_{ij}|)$ are used in the derivations.

Theorem 1: Given $\mathbf{w}^{(0)} = \mathbf{x}$, $\|\mathbf{w}\|_\infty = w_b < 1$, and provided that $D\mathbf{g}(\mathbf{w})$ (the Jacobian of $\mathbf{g}$ at $\mathbf{w}$) is non-singular, then,

$$\mathbf{w}^{(k+1)} \triangleq \mathbf{w}^{(k)} - D\mathbf{g}(\mathbf{w}^{(k)})^{-1}\left[\mathbf{g}(\mathbf{w}^{(k)}) - \mathbf{x}\right] \tag{7}$$

is well defined for $k = 0, 1, \ldots$. Also $\lim_{k\to\infty} \mathbf{w}^{(k)} = \mathbf{w}^*$ such that $\mathbf{g}(\mathbf{w}^*) - \mathbf{x} = 0$. Finally for all $k \ge 0$

$$\|\mathbf{w}^{(k)} - \mathbf{w}^*\|_\infty \le \alpha \frac{h^{2^k - 1}}{1 - h^{2^k}}, \tag{8}$$

where

$$\alpha = \sec\left(\frac{\pi w_b}{2}\right)\left[w_b - \frac{2}{\pi}\operatorname{Si}\left(\frac{\pi w_b}{2}\right) + \mu\right]$$

with $0 < \mu < 0.236$ for $0 < w_b < 1$ (see (14), Appendix A), and

$$h = \frac{\alpha}{2w_b}\left[\frac{\operatorname{sinc}(\frac{w_b}{2})}{\cos(\frac{\pi w_b}{2})} - 1\right].$$

Proof: See Appendix A-A. ∎

Theorem 1 guarantees the convergence of the recursion. Starting it with an initial guess $\mathbf{w}^{(0)} = \mathbf{x}$ (i.e., the duty-cycle values of the classical SDEUPWM modulation described in Section II), ensures the convergence in fewer steps because the starting point is closer to $\mathbf{w}^*$. The theorem also provides a bound for the difference between the duty-cycles at iteration k and the duty-cycles $\mathbf{w}^*$ that achieve zero distortion.

The next theorem establishes a bound on the maximum baseband error, given by the maximum difference between $\mathbf{x}$ (the samples of the modulating signal) and $\mathbf{y}^{(k)}$ (the samples of the filtered PWM at iteration $k > 0$). It also demonstrates that a slight correction in the duty-cycles produces a significant reduction in the baseband distortion.

Theorem 2: If $\|\mathbf{w}\|_\infty = w_b < 1$, then

$$\|\mathbf{y}^{(k)} - \mathbf{x}\|_\infty \le \frac{\gamma}{2}\|\mathbf{w}^{(k)} - \mathbf{w}^*\|_\infty^2 \le \frac{\gamma\alpha^2}{2}\left(\frac{h^{2^k-1}}{1-h^{2^k}}\right)^2 \tag{9}$$

where $\gamma < 1$ is given by

$$\gamma = \frac{1}{w_b}\left[\operatorname{sinc}\left(\frac{w_b}{2}\right) - \cos\left(\frac{\pi w_b}{2}\right)\right] \in \left(0, \frac{2}{\pi}\right)$$

for $0 < w_b < 1$.

Proof: See Appendix A-B. ∎

B. Applications

Theorems 1 and 2 can be helpful at the design stage. For example, if the designer fixes the maximum number of iterations due to limited processing capabilities, Theorem 1 establishes the maximum difference between the duty cycle at the k-th iteration and the limit $\mathbf{w}^*$. This value is useful to set the resolution of the PWM: the number of bits b must be chosen so that the distance $\|\mathbf{w}^{(k)} - \mathbf{w}^*\|_\infty > 2^{-b}$, i.e., it is within the resolution

of the PWM. Theorem 2 provides a bound on the maximum sample error $\|\mathbf{y}^{(k)} - \mathbf{x}\|_\infty$ that is attainable with this design. In other scenario, the designer chooses to achieve a given maximum sample error $\|\mathbf{y}^{(k)} - \mathbf{x}\|_\infty$. Theorem 2 establishes the number k of iterations required, and Theorem 1 can be used to estimate the resolution of the PWM.

Examples: Assuming a maximum duty-cycle $w_b = 1/2$ results in $\alpha = 0.07$, $h = 0.02 < 1$ and $\gamma = 0.39$. As an example of the first scenario, if the designer chooses to perform only one iteration ($k = 1$), (9) in Theorem 2 shows that the maximum sample error satisfies $\|\mathbf{y}^{(1)} - \mathbf{x}\|_\infty < 1 \times 10^{-3}$. For SDEUPWM modulation this error is $\|\mathbf{y}^{(0)} - \mathbf{x}\|_\infty \leq 50 \times 10^{-3}$ (see Lemma 2 in Appendix A). Therefore, a single iteration of the algorithm is capable of reducing the worst case error at least 50 times; RMS distortion levels are usually even smaller. From Theorem 1 the maximum difference between the corrected duty-cycles and the limit $\mathbf{w}^*$ is given by (8): $\|\mathbf{w}^{(1)} - \mathbf{w}^*\|_\infty < 1.36 \times 10^{-3}$ that can be resolved using a PWM counter of at least $b = 10$ bits.

On the other hand, if the designer specifies a maximum error sample value $\|\mathbf{y}^{(k)} - \mathbf{x}\|_\infty < 0.35 \times 10^{-6}$, (9) in Theorem 2 shows that this value can be achieved with $k = 2$ iterations. From Theorem 1 using (8) it is found that $\|\mathbf{w}^{(2)} - \mathbf{w}^*\|_\infty < 0.51 \times 10^{-6}$ that results in a PWM counter with at least $b = 21$ bits. This is a large value for practical applications; however, there are several alternatives to achieve high PWM resolution without requiring high frequency clocks, see for example [20], Table I for a DSP platform and [21], [22] for FPGAs.

IV. Architecture for Real-Time Implementation

In the previous section the computation of the duty-cycles w_n to achieve perfect reconstruction of finite length signals was addressed. However, its application requires the knowledge of the entire vector $\mathbf{x}$ of samples of the modulating signal, and therefore it is not suitable for on-line applications, especially when N is large. In this section, the problem of computing the duty-cycles of arbitrary long signals (large N) using shorter segments of length $L \ll N$ is solved using block processing techniques.

The result of the first iteration in (7), namely $\mathbf{w}^{(1)}$ is used to estimate the corrected duty-cycles $\mathbf{w}^*$ for each block. These modifications significantly reduce the computational requirements of the algorithm, making it feasible for a real-time implementation. Error bounds due to block-length effects are also derived.

A. Block Processing Architecture

The block processing architecture is based on overlapped serial to parallel (SP) and parallel to serial (PS) converters [Fig. 1(a)]. The SP and PS blocks can be easily constructed using tapped delays, L downsampling-by-M blocks, and P upsampling-by-M blocks, respectively, with $M \leq \min(L, P)$. These blocks are typically used in multirate systems (see for example [23]) but other algorithms can also be used to stitch the successive overlapped blocks of an arbitrary long signal. A block vector $\mathbf{x}_L^M[n]$ is defined as

$$\mathbf{x}_L^M[n] = [x_{nM}, x_{nM-1}, \ldots, x_{nM-L+1}]^T,$$

i.e., it is composed of L consecutive samples taken every M samples. If $L = M$ there is no overlap, but if $L > M$ the last $(L - M)$ samples of $\mathbf{x}_L^M[n]$ overlap with the first $(L - M)$ samples of $\mathbf{x}_L^M[n-1]$.

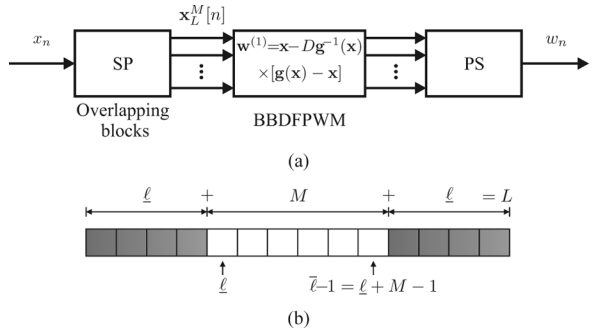

Fig. 1. Architecture for the block processing PWM algorithm.

The last configuration is chosen for the block implementation of the baseband distortion-free PWM (BBDFPWM) algorithm shown in Fig. 1(a), using L consecutive samples of the modulating signal to compute M duty-cycles, and discarding $\underline{\ell} = (L - M)/2$ samples at the edges of each block to reconstruct the one-dimensional signal with the PS block. A block of length L of the modulating signal is shown in Fig. 1(b), where the discarded samples are indicated with gray boxes. Without loss of generality, we assume that $L - M$ is even.

B. Block Processing Errors

When duty-cycles are computed using the block processing architecture described above, certain error in the calculation of y_n has to be expected because only L samples instead of N are used in (6). In the following its dependence with the values of L and M is analyzed.

The samples of the filtered PWM signal computed with the block processing architecture will be noted as $\breve{y}_n$. In each block, M duty-cycles w_n, with $n \in [\underline{\ell}, \overline{\ell}-1]$, and $\overline{\ell} \triangleq (L+M)/2$, have to be computed using L samples of the modulating signal, since $\underline{\ell}$ samples at each edge of the block are discarded. The block processing error is defined as $e_B = \|y_n - \breve{y}_n\|_\infty$ and achieves its maximum value at $n = \underline{\ell}$ and/or $n = \overline{\ell} - 1$ because all samples at the left or right side, respectively, are discarded as shown in Fig. 1(b). A bound over e_B is provided by the following Theorem.

Theorem 3: The block processing error e_B is bounded by $e_B \leq \overline{e}_B$ where

$$\overline{e}_B = \mu + \sum_{k=1}^{\overline{\ell}-1} (-1)^k f_k(w_b) + \sum_{k=1}^{\underline{\ell}} (-1)^k f_k(w_b), \qquad (10)$$

where $f_k(\cdot)$ is given by (5), $w_b = \|\mathbf{w}\|_\infty < 1$ and μ is given by (14) (see Appendix A).

Proof: See Appendix A-C. ∎

A representation of $\overline{e}_B$ as a function of L, M/L and parametrized for three different values of w_b is shown in Fig. 2. The surface plot shows that the bock processing error can be reduced by either augmenting the block length L, or by dropping out a large number of samples (M/L small). It can also be noted that the rate of error reduction decreases for $L > 60$, and for $M/L < 0.15$. A good compromise between algorithm complexity and block processing error may be obtained when selecting parameters M, L to lie within this range. However, the surface plot reveals that the main factor for reducing the block processing error is a small bound w_b on the maximum value of the duty-cycle. In practical applications, this may be a con-

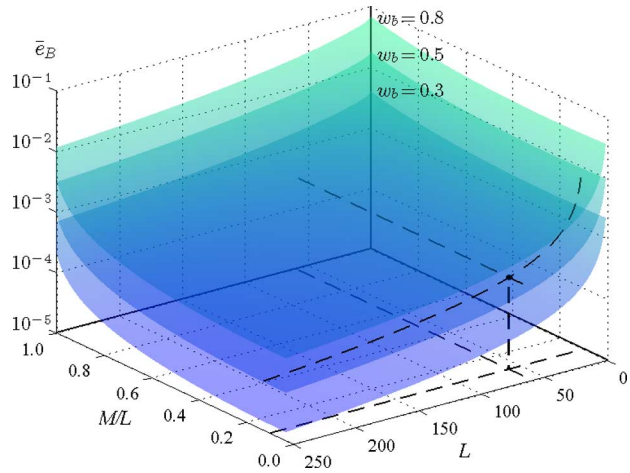

Fig. 2. Maximum block processing error $\bar{e}_B$ as a function of M/L and L, for $w_b = 0.3$, 0.5, and 0.8.

flicting requirement due to reduced switch and bus voltage utilization in power applications and the finite resolution of the PWM pulse width in digital implementations.

C. Algorithm Complexity and Implementation Alternatives

The computation of the corrected duty-cycle is a two-step procedure: the computation of the Newton's correction term and the calculation of the demodulated signal samples. A straightforward implementation of the former, given by (7), is computationally intensive but several alternatives can be considered to lower the computational cost. A numerical analysis of the Jacobian matrix, whose elements are computed by (12) (See Appendix A), reveal that it is diagonal dominant, justifying the use of incomplete Jacobian Newton (IJN) methods [24]. An invertible matrix $H(\mathbf{w}^{(k)})$ is defined as

$$[H(\mathbf{w}^{(k)})]_{i,j} = \begin{cases} [D\mathbf{g}(\mathbf{w}^{(k)})]_{i,j}, & \text{if } i,j \in \mathbf{c}^{(k)}, \\ 0, & \text{otherwise,} \end{cases}$$

where $\mathbf{c}^{(k)}$ is an index set. The convergence properties of the IJN method depends on the selection of $\mathbf{c}^{(k)}$ [24]. The procedure required to implement (7) using $H(\mathbf{w}^{(k)})$ as an approximation to the Jacobian is listed as a pseudo-code in Algorithm 1. Some alternatives on the election of the index set $\mathbf{c}^{(k)}$ are discussed next.

Algorithm 1 Duty-cycle computation: pseudo-code

Require: $\mathbf{x} \in \mathbb{R}^L$: vector of modulating signal samples
  $\mathbf{w}^{(0)} \leftarrow \mathbf{x}$
  for $i = 1$ to N_i **do**
    for $n = \underline{\ell}$ to $\overline{\ell} - 1$ **do**
      $y_n \leftarrow [\mathbf{g}(\mathbf{w}^{(i-1)})]_n$ using (11).
    end for
    Update $H(\mathbf{w}^{(i-1)})$ using the chosen Jacobian method
    $\mathbf{w}^{(i)} \leftarrow \mathbf{w}^{(i-1)} - H(\mathbf{w}^{(i-1)})^{-1}(\mathbf{g}(\mathbf{w}^{(i-1)}) - \mathbf{x})$
  end for

1) Full Jacobian: Computation of the inverse of the Jacobian using Gauss-Jordan elimination has a complexity of $\mathcal{O}(L^3)$. Alternatively, $(D\mathbf{g})^{-1}$ can be computed as a finite number of terms of its power expansion series, $(D\mathbf{g})^{-1} \approx I + (I - D\mathbf{g}) + (I - D\mathbf{g})^2$ (see Appendix A), but complexity remains $\mathcal{O}(L^3)$ because of the square on $D\mathbf{g}$.

2) Tridiagonal Jacobian: A strong reduction in computational complexity to $\mathcal{O}(L)$, while preserving good convergence characteristics is achieved by choosing $H(\mathbf{w}^{(k)})$ as a tridiagonal matrix [25]. The three main diagonals of the Jacobian $D\mathbf{g}$ are preserved while the other elements are set to zero.

3) Diagonal Jacobian: In this case $H(\mathbf{w}^{(k)})$ is composed of the main diagonal of the Jacobian $D\mathbf{g}$. Its inverse is $[H(\mathbf{w}^{(k)})^{-1}]_{j,j} = \text{sinc}(w_j/2)^{-1}$, resulting in $\mathcal{O}(1)$ complexity.

4) Jacobian Free: As an alternative to the previous approximations, $H(\mathbf{w}^{(k)})$ could be set to a constant diagonal matrix [26] setting also the complexity order to $\mathcal{O}(1)$ but without the need for computing any element of the Jacobian matrix.

In addition to the computation of the Jacobian using any of the methods described above, Algorithm 1 also requires the evaluation of $y_n = [\mathbf{g}(\mathbf{w}^{(0)})]_n$ using (6) as a starting point of the iterative procedure. This is a nonlinear function of the duty-cycles $\mathbf{w}$. To further reduce the computational cost, $f_k(w)$ in (6) is approximated using (17) (see Appendix B), and therefore each demodulated signal sample y_n can be computed as

$$y_n = \sum_{k=0}^{L-1} \left(h_{1,k} w_{n-k} + h_{3,k} w_{n-k}^3 + h_{5,k} w_{n-k}^5 + h_{7,k} w_{n-k}^7 \right). \tag{11}$$

Number of Multiplications and Iterations: The largest number of operations per sample required to compute y_n using (11) may be estimated as follows. Setting $M = 1$ (assuming that L is odd) results in the computation of just a single duty-cycle in each iteration, namely the sample $n = \underline{\ell} = (L-1)/2 = \overline{\ell} - 1$. Since $h_{1,k}$ is non zero only for $k = \underline{\ell}$ and $h_{3,k}$, $h_{5,k}$ and $h_{7,k}$ are symmetric around $k = \underline{\ell}$ (see Appendix B), the computation of each demodulated signal sample y_n demands only $4 + 3\underline{\ell}$, resulting in $\mathcal{O}(L)$ complexity.

The approximated Jacobian methods described above may require more than one iteration to increase the SNR by an amount equivalent to that achieved by a single iteration of the full Newton algorithm. However, even with two or three iterations the number of operations required by these methods is still much lower than those required by the full Jacobian. Table I shows the increase of the SNR as a function of the number of iterations N_i obtained for a random band limited signal with different Jacobian computation alternatives. This Table shows that the diagonal Jacobian algorithm with three iterations ($N_i = 3$) results in a good a compromise between performance and computational load, and therefore it is chosen for the experiences studied in Section V.

TABLE I
SNR AND COMPLEXITY OF IMPLEMENTATION ALTERNATIVES

Jacobian	SNR [dB]			Complexity
	$N_i = 1$	$N_i = 2$	$N_i = 3$	
Full	117	167	237	$\mathcal{O}(L^3)$
Tridiagonal	79.85	122	160	$\mathcal{O}(L)$
Diagonal	68.79	101	128	$\mathcal{O}(1)$
Free	65.22	87.56	109	$\mathcal{O}(1)$

The total number of multiplications per duty-cycle required by this method, including the Jacobian approximation and the computation of the sample of the demodulated signal, is given by

$$\mathcal{M} = N_i \left[4 + \frac{3}{2}(L-1)\right] + N_i,$$

where N_i is the number of iterations, $4 + 3(L-1)/2$ is the number of multiplications required to compute y_n with (11) in each iteration and the last N_i multiplications accounts for the product between the Newton correction term and the error: $H(\mathbf{w}^{(i-1)})^{-1}(\mathbf{g}(\mathbf{w}^{(i-1)}) - \mathbf{x}) = [\mathrm{sinc}(w_n/2)]^{-1}(y_n - x_n)$.

V. Examples

In this section the performance of the algorithm is evaluated using different band-limited signals. In the first set of signals, the maximum amplitude of the modulating signal is limited to 0.8 of the amplitude constraint $2/\pi$ [18], resulting in $w_b \approx 0.5$. In the last example, the algorithm is tested with a signal which does not satisfies this constraint.

To quantify the performance of the algorithm two indices are computed: e_{RMS}, the RMS value of the error $(x_n - y_n)$, and the signal to noise ratio,

$$\mathrm{SNR} = 20\log_{10}\left(\frac{x_{\mathrm{RMS}}}{e_{\mathrm{RMS}}}\right),$$

where x_{RMS} is the RMS value of x_n.

Tests were performed using a normalized sampling and PWM frequencies of $f_s = 1$, and the following modulating signals: 1) low and 2) high frequency sinusoids, 3) filtered random noise, and 4) intermodulation distortion (IMD) test signals. A fifth test signal, composed of a short segment of a musical score, was also used to test the performance of the algorithm when the amplitude limit is violated. In the first and second cases, the frequency is chosen as 20% and 80% of the of the Nyquist frequency $f_s/2$. The third signal is random noise with normal distribution and band-pass filtered between 5.7×10^{-3} and 0.272 of the sampling frequency (corresponding to 250 Hz and 12 kHz for $f_s = 44.1$ kHz). The fourth signal follows DIN standard 45403 for IMD measurements, widely used in the broadcast and consumer audio fields. It is composed of low and high frequency sinusoids (usually 250 Hz and 8 kHz), where the latter has an amplitude 12.04 dB lower than the former. For a sampling frequency of 44.1 kHz, the normalized frequencies are 5.7×10^{-3} and 0.181, respectively.

In the following, the performance of the BBDFPWM algorithm is compared to the SDEUPWM modulation described in Section II.

A. Block Processing Error

The theoretical bound of the block processing error given by (10) is depicted as a function of half the number of discarded samples $\underline{\ell} = (L-M)/2$ in Fig. 3 for $w_b = 0.5$ (continuous curve) and $w_b = 1$ (dashed curve). The actual error values for the four test signals described above (with $w_b = 0.5$) are also shown; the vertical dotted line indicates the operating point chosen for the examples ($L = 60, M = 6$). Although the theoretical bound (10) is conservative, the closest signal to this bound is the high frequency sinusoid because the contribution of the discarded samples in (6) is higher when the ratio f_m/f_s approaches $1/2$.

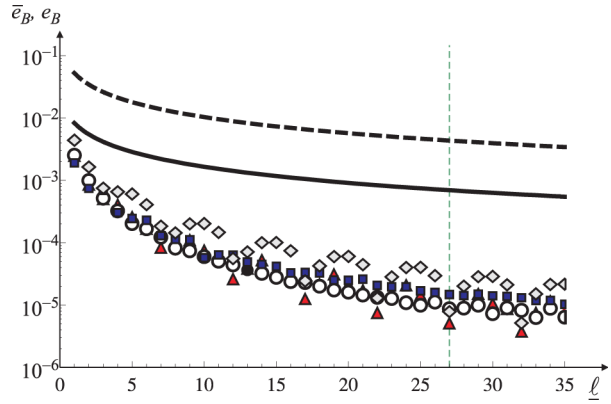

Fig. 3. Block processing error bound $\bar{e}_B$ as a function of $\underline{\ell} = (L-M)/2$ for $M = 6$: $w_b = 0.5$(—); $w_b = 1$(- -). Also shown are actual error values e_B for typical signals: (red ▲) low frequency sinusoid; (gray ♦) high frequency sinusoid; (blue ■) filtered random noise; (black ●) two-tone IMD signal. The vertical dotted line indicates the operating point chosen in Section V.

B. Spectral Analysis

The effects of the block length L, the approximate Jacobian and the finite number of iterations N_i on the spectral characteristic of the BBDFPWM algorithm are addressed experimentally in this section. For this study, the block length is fixed at $L = 60$, with $\underline{\ell} = (L-M)/2 = 27$ samples discarded at both ends of the block. Therefore, $M = 6$ samples are retained for non-overlapped reconstruction. This operating point is indicated with a dot in Fig. 2 and a thin dotted vertical line in Fig. 3, and it is comprised within the operating region suggested in Section IV-B.

Figs. 4–7 show the spectra for the four signals under analysis[2]. The dashed line at $f_s/2 = 0.5$ indicates the upper baseband limit. For comparison purposes, the spectra for both BBDFPWM and SDEUPWM are depicted.

Fig. 4 depicts the spectrum of the PWM signal when the modulating signal is a low frequency sinusoid of frequency $f_m = 0.1 f_s$. The advantages of the proposed modulation scheme are revealed by the absence of any relevant harmonic component other than the fundamental within the baseband. The BBDFPWM achieves a SNR of 96.44 dB, while SDEUPWM achieves only 40 dB due to the presence of the third and fifth harmonics as described by (2). The RMS error is reduced from 3.6×10^{-3} to 5.42×10^{-6}.

Fig. 5 depicts the spectrum of the high frequency sinusoid of frequency $f_m = 0.4 f_s$. The increase in the SNR is larger than in the previous example raising from 25.94 dB for SDEUPWM to 90 dB for BBDFPWM, mainly due to the elimination of the subharmonic component at $0.2 f_s$. The RMS error reduces from 18.2×10^{-3} to 12.3×10^{-6}.

For the filtered random noise (signal 3) the SDEUPWM modulation exhibits distortion that extends beyond the Nyquist frequency $f_s/2 = 0.5$ as shown in Fig. 6, with a noise floor in excess of -50 dB. This baseband distortion is caused by the term

[2]The spectra are obtained via FFT computation. After filtering the continuous $p(t)$ PWM signal with an 8-th order low-pass filter with cut-off frequency $4f_s$ to avoid aliasing, the signal is sampled at 1000 f_s and then time-windowed to prevent spectral leakage and picket-fence effects [27]. In an actual measurement set-up all these operations are performed by the input stage of a spectrum analyzer.

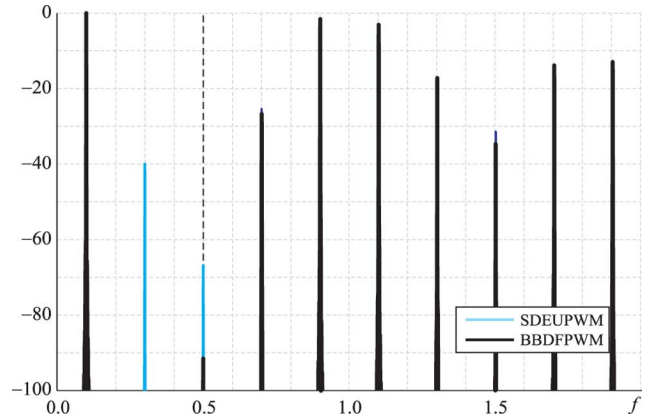

Fig. 4. Frequency spectrum of the modulated signal. Modulating signal 1: sinusoidal of frequency $f_m = 0.1 f_s$.

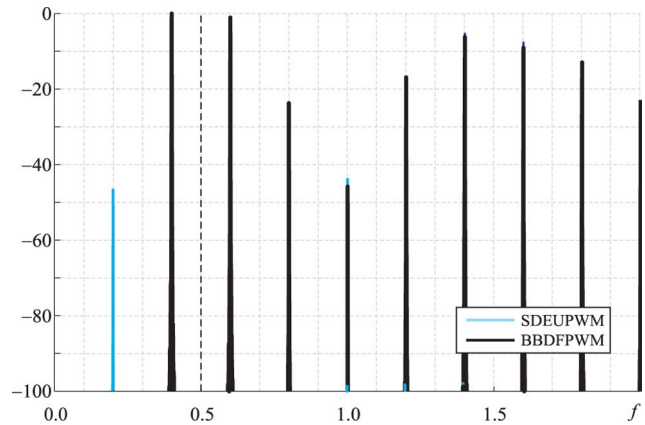

Fig. 5. Frequency spectrum of the modulated signal. Modulating signal 2: sinusoidal near Nyquist frequency, $f_m = 0.4 f_s$.

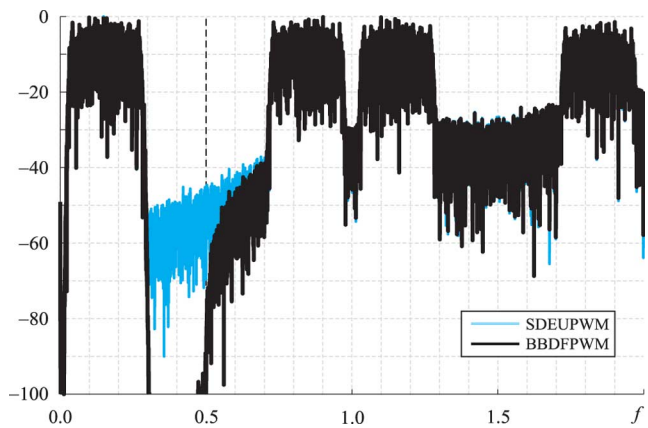

Fig. 6. Frequency spectrum of the modulated signal. Modulating signal 3: band-limited random noise.

$X_1(f)$ in (2), and it virtually disappears for the BBDFPWM modulator. The SNR increases from 45.43 dB for SDEUPWM to 99.24 dB for BBDFPWM and the RMS error is reduced from 0.59×10^{-3} to 1.20×10^{-6}.

The spectrum of the standard IMD test (signal 4) depicted in Fig. 7 also shows the high performance of BBDFPWM modulation. The SDEUPWM spectrum (SNR $= 45.43$ dB) exhibits undesired side-bands around $f_{m2} = 0.18$ with an amplitude of -55 dB, but two other unwanted frequency components of similar amplitude appear near $0.37 f_s$ and a last component of nearly -70 dB at $0.45 f_s$. These spurious tones are completely removed by BBDFPWM modulation (SNR=97.38 dB), revealing its higher linearity. The RMS error is reduced from 1.4×10^{-3} to 4.02×10^{-6}.

Although BBDFPWM should not exhibit harmonic distortion in the baseband, it is expected that some distortion components may appear because of the approximate solution of Algorithm 1 and the error caused by block processing. However, in the spectra of the two first examples (Figs. 4 and 5) no distortion components can be observed. Only in the last two examples, the error of the BBDFPWM algorithm are revealed by a small frequency component (below -95 dB) near the boundary of the baseband ($f = 0.5$).

These results are summarized in Table II, that lists the SNR for both BBDFPWM and SDEUPWM. The proposed modulation method is able to increase the SNR by at least 50 dB. For each of the signals of the previous examples the mean and maximum pulse width variation among SDEUPWM and BBDFPWM ($\Delta w_{\text{avg}}\% = 100 \operatorname{avg} |\mathbf{w}^{(i)} - \mathbf{w}^{(0)}|$, $\max(\Delta w)\% = 100 \max |\mathbf{w}^{(i)} - \mathbf{w}^{(0)}|$, respectively) were also computed. It is noticeable that such performance enhancement can be achieved by minimum adjustments of the PWM pulse width values. These results, however, are in accordance with the postulates of Theorems 1 and 2.

C. A Practical Case Not Satisfying $2/\pi$ Constraint

The proposed BBDFPWM algorithm was also tested using a real audio signal (the song "Like a Rolling Stone" from Bob Dylan), also analyzed in [19]. The signal is sampled at 44.1 kHz with a resolution of 16 bits and the PWM frequency is also set to $f_s = 44.1$ kHz.

The maximum value of the modulating signal $\|\mathbf{x}\|_\infty = A_m = \max(|x_n|)$ was varied between 0.5 and 1. The amplitude constraint is violated when $A_m > 2/\pi \approx 0.64$. The maximum amplitude limit is set to $A_m < 1$ to avoid undesired overmodulation in SDEUPWM. The parameters of the BBDFPWM are: block length $L = 59$, diagonal Jacobian algorithm with three iterations ($N_i = 3$), and a single duty-cycle recovered from each block ($M = 1$). The histogram of the signal, depicted in Fig. 8(a), shows that the distribution of the amplitudes is approximately Gaussian (solid curve, with zero mean and variance $\sigma^2 = 0.041$). The signal at full modulation index ($A_m = 1$) is shown in Fig. 8(b), where the $2/\pi$ bound is indicated with a dashed line. Fig. 8(c) shows that the SNR for BBDFPWM and SDEUPWM decreases with increasing values of A_m. However, the SNR of the BBDFPWM clearly outperforms the SDEUPWM by nearly 40 dB, even when the amplitude constraint is not honored.

The BBDFPWM algorithm also compares favorably with similar approaches in the literature. For example, in [19] a discrete-time Volterra prefilter was employed to reduce distortion in PWM applications. Using this same test signal, with $A_m = 0.9$, both approaches are able to achieve a SNR above 90 dB. However, this performance is reached with only 276 multiplications per duty-cycle when using the BBDFPWM modulator, and rises to 1342 multiplications per duty-cycle (485% higher) for the Volterra prefilter.

VI. Conclusion

A PWM algorithm capable of achieving high signal to noise ratios (in excess of 90 dB) for bounded, band-limited

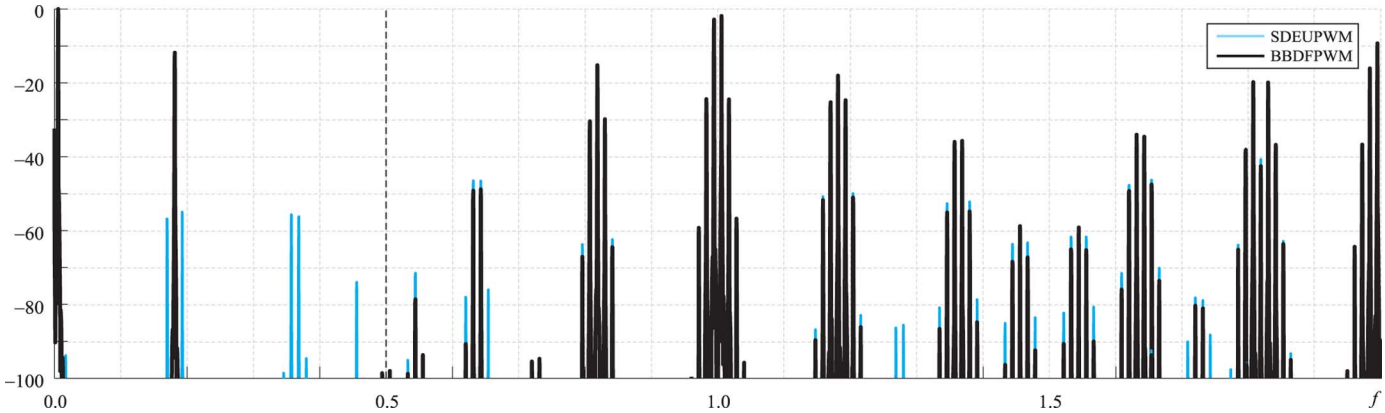

Fig. 7. Frequency spectrum of the modulated signal. Modulating signal 4: IMD test.

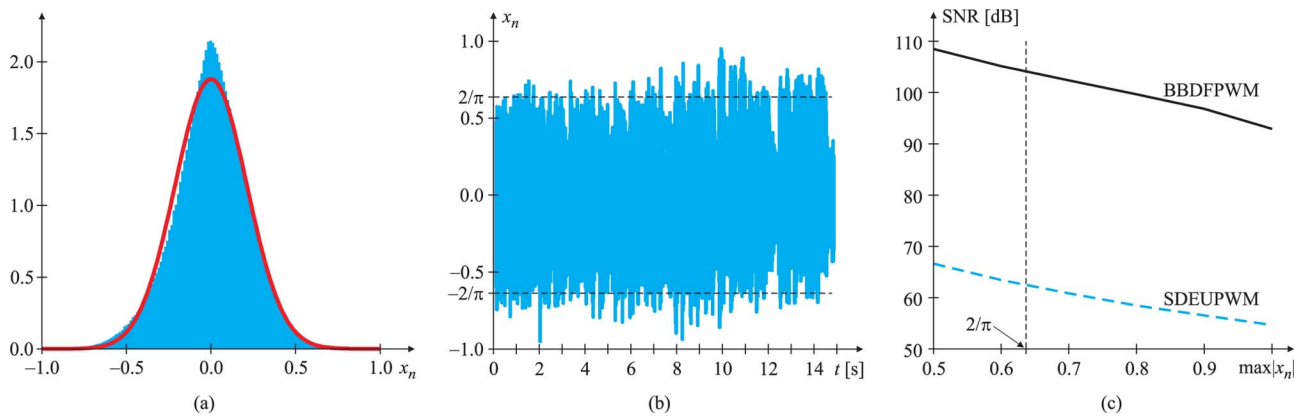

Fig. 8. Audio signal experiment: (a) histogram; (b) time domain; (c) SNR as a function of $A_m = \max(|x_n|)$ for BBDFPWM (—) and SDEUPWM (–).

TABLE II
BASEBAND SNR AND DUTY-CYCLE VARIATION

Test	SNR [dB]		$\Delta w_{\text{avg}}\%$	$\max(\Delta w)\%$
	BBDFPWM	SDEUPWM		
1 (Fig.4)	96.44	40.00	0.30	1.36
2 (Fig.5)	90.00	25.94	1.90	3.33
3 (Fig.6)	99.24	45.43	0.09	1.64
4 (Fig.7)	97.38	46.59	0.11	0.46

signals was developed in this paper. The method is suitable for real-time operation by using block processing techniques. Newton method is employed to approximately invert the non-linear mapping produced by the PWM modulation, and explicit error bounds for the different approximations are given. This modulator greatly increases the SNR for typical signals with respect to standard PWM modulators. The low switching frequency at which the algorithm can operate allows to reduce switching losses, and may enable the use of switching amplifiers for applications where a high ratio between the frequency of the carrier and modulating signal is prohibitive.

APPENDIX A
THEOREMS' PROOFS

To simplify the notation, we define the function $\boldsymbol{\rho}(\mathbf{w}) \triangleq \mathbf{g}(\mathbf{w}) - \mathbf{x}$. The Jacobian of $\boldsymbol{\rho}$ will be noted as $D\boldsymbol{\rho}$ and $D\boldsymbol{\rho} = D\mathbf{g}$, where each element of $\mathbf{g}(\mathbf{w})$ is given by (6). Using (6), the (i, j) element of $D\boldsymbol{\rho}(\mathbf{w})$ is given by

$$D\boldsymbol{\rho}(\mathbf{w})_{i,j} = \frac{dg_i(\mathbf{w})}{dw_j} = \frac{df_{i-j}(w_j)}{dw_j} = f'_{i-j}(w_j). \tag{12}$$

The derivative of $f_m(w)$ w.r.t. w for all $m \geq 0$ is

$$f'_m(w) = \frac{\left[\operatorname{sinc}\left(\frac{m-w}{2}\right) + \operatorname{sinc}\left(\frac{m+w}{2}\right)\right]}{2}. \tag{13}$$

The term $\sum_{k=1}^{\infty} f_k(w_{n-k}) + f_k(w_{n+k})$ in (4) can be interpreted as the contribution of the other duty-cycles to the current demodulated signal sample. It is bounded by $\mu(w_b)$, a function of the maximum duty-cycle $0 < w_b < 1$:

$$\mu(w_b) \triangleq 2 \sum_{m=1}^{\infty} (-1)^{1+m} f_m(w_b). \tag{14}$$

Its maximum value is $\mu_{\max} \approx 0.236$ for $w_b = 1$ [18]. With these definitions, the recursion (7) can be written as

$$D\boldsymbol{\rho}(\mathbf{w}^{(i)})\Delta\mathbf{w}^{(i)} = -\boldsymbol{\rho}(\mathbf{w}^{(i)}),$$
$$\mathbf{w}^{(i+1)} = \mathbf{w}^{(i)} + \Delta\mathbf{w}^{(i)}.$$

Some results for $\boldsymbol{\rho}$ and its Jacobian $D\boldsymbol{\rho}$ follows.

Lemma 1: $D\boldsymbol{\rho}$ is Lipschitz and $D\boldsymbol{\rho}^{-1}$ is bounded.

Proof: The maximum value of the second derivative of $f_m(w)$ can be found taking the derivative of (13) and evaluating it at $m = 0$, yielding

$$\begin{aligned}\|D\boldsymbol{\rho}(\mathbf{u}) - D\boldsymbol{\rho}(\mathbf{v})\|_{\infty_i} &\leq \max_{m;w}\left\{\frac{d^2}{dw^2}g_m(w)\right\}\|\mathbf{u}-\mathbf{v}\|_\infty \\ &= \gamma\|\mathbf{u}-\mathbf{v}\|_\infty\end{aligned}$$

where $\gamma \triangleq [2/(\pi w_b^2)]\sin(\pi w_b/2) - (1/w_b)\cos(\pi w_b/2)$ ranges between $0 < \gamma < 2/\pi$ for $0 < w_b < 1$. It can also be shown that

$$\begin{aligned}&\|(I - D\boldsymbol{\rho})\|_{\infty_i} \\ &= \max_{1\leq n\leq N}\sum_{m=1}^{N}|[I - D\boldsymbol{\rho}]_{n,m}| \\ &= \max_{1\leq n\leq N}[1 - f_0'(w_n) + \sum_{m=-(n-1);m\neq 0}^{N-n}|f_m'(w_{n+m})|] \\ &\leq 1 - f_0'(w_b) + 2\sum_{m=1}^{\infty}f_m'(w_b)(-1)^{m+1} \\ &= 2\sin\left(\frac{\pi w_b}{4}\right)^2, \qquad (15)\end{aligned}$$

which is less than one for $0 < w_b < 1$. Using Newman series and (15), it can be shown that $D\boldsymbol{\rho}^{-1}$ is bounded by

$$\|D\boldsymbol{\rho}^{-1}\|_{\infty_i} \leq \|I\|_{\infty_i} + \sum_{n=1}^{\infty}\|I - D\boldsymbol{\rho}\|_{\infty i}^n = \sec\left(\frac{\pi w_b}{2}\right) \triangleq \beta.$$

■

Lemma 2: The vector $\boldsymbol{\rho}(\mathbf{w}^{(0)})$ is bounded.

Proof: From the definition

$$\begin{aligned}\|\boldsymbol{\rho}(\mathbf{w}^{(0)})\|_\infty &= \|\mathbf{g}(\mathbf{x}) - \mathbf{x}\|_\infty \\ &= \max_j(|\,[\mathbf{g}(\mathbf{x})]_j - [\mathbf{x}]_j\,|)\end{aligned}$$

where we used that $\mathbf{w}^{(0)}$ coincides with the samples $\mathbf{x}$ that are equal to the desired demodulated signal. On the other hand

$$\begin{aligned}&|\,[\mathbf{g}(\mathbf{x})]_j - [\mathbf{x}]_j\,| \\ &= |g_j(\mathbf{x}) - x_j| \\ &= |f_0(x_j) + \sum_{k=1}^{N-1-n}f_k(x_{j+k}) + \sum_{k=1}^{n}f_k(x_{j-k}) - x_j| \\ &\leq |f_0(x_j) - x_j| + \mu \\ &\leq w_b - \frac{2}{\pi}\,\mathrm{Si}\left(\frac{\pi w_b}{2}\right) + \mu\end{aligned}$$

and hence $\|\mathbf{g}(\mathbf{x}) - \mathbf{x}\|_\infty \leq w_b - (2/\pi)\,\mathrm{Si}\,(\pi w_b/2) + \mu$. ■

Lemma 3: If $D\boldsymbol{\rho}(\mathbf{w})$ is well defined for all $\mathbf{w}$ in a convex region $C_0 \subseteq \mathbb{R}^n$ and

$$\|D\boldsymbol{\rho}(\mathbf{u}) - D\boldsymbol{\rho}(\mathbf{v})\|_{\infty_i} \leq \gamma\|\mathbf{u}-\mathbf{v}\|_\infty \;\forall \mathbf{u},\mathbf{v}\in C_0,$$

then

$$\|\boldsymbol{\rho}(\mathbf{u}) - \boldsymbol{\rho}(\mathbf{v}) - D\boldsymbol{\rho}(\mathbf{v})(\mathbf{u}-\mathbf{v})\|_\infty \leq \frac{\gamma}{2}\|\mathbf{u}-\mathbf{v}\|_\infty^2.$$

Proof: See [25], pages 269–270. ■

Theorem 4: Given an open set $C \subseteq \mathbb{R}^n$ and a convex set C_0 such that $\overline{C}_0 \subseteq C$. Given the differentiable function $\boldsymbol{\rho} : C \to \mathbb{R}^n \;\forall\, \mathbf{w} \in C_0$ and continuous for $\mathbf{w} \in C$, let $S_r(\mathbf{w}^{(0)}) \triangleq \{\mathbf{w} : \|\mathbf{w} - \mathbf{w}^{(0)}\|_\infty < r\} \in C_0$, $h \triangleq \alpha\beta\gamma/2 < 1$ and $r \triangleq \alpha/(1-h)$. If $D\boldsymbol{\rho}$ is Lipschitz: $\|D\boldsymbol{\rho}(\mathbf{w}) - D\boldsymbol{\rho}(\mathbf{v})\|_{\infty_i} \leq \gamma\|\mathbf{w}-\mathbf{v}\|_\infty$ and $\|\,(D\boldsymbol{\rho}(\mathbf{w}))^{-1}\,\|_{\infty_i} \leq \beta$ and $\|\,\left(D\boldsymbol{\rho}(\mathbf{w}^{(0)})\right)^{-1}\boldsymbol{\rho}(\mathbf{w}^{(0)})\|_{\infty_i} \leq \alpha$, then the recursion

$$\mathbf{w}^{(k+1)} \triangleq \mathbf{w}^{(k)} - \left(D\boldsymbol{\rho}(\mathbf{w}^{(k)})\right)^{-1}\boldsymbol{\rho}(\mathbf{w}^{(k)})$$

is well defined for $k = 0, 1, \ldots$ and verifies $\mathbf{w}^{(k)} \in S_r(\mathbf{w}^{(0)})\;\forall\, k \geq 0$. Also $\lim_{k\to\infty}\mathbf{w}^{(k)} = \xi$ such that $\boldsymbol{\rho}(\xi) = 0$. Finally for all $k \geq 0$

$$\|\mathbf{w}^{(k)} - \xi\|_\infty \leq \alpha\frac{h^{2^k-1}}{1-h^{2^k}}.$$

Proof: See [25], pages 270–272. ■

A) Proof of Theorem 1:

Proof: The demonstration is straightforward. From Lemma 1 and Lemma 2,

$$\begin{aligned}\|D\boldsymbol{\rho}(\mathbf{w}^{(0)})^{-1}\boldsymbol{\rho}(\mathbf{w}^{(0)})\|_\infty &\leq \|D\boldsymbol{\rho}(\mathbf{w}^{(0)})^{-1}\|_{\infty_i}\|\boldsymbol{\rho}(\mathbf{w}^{(0)})\|_\infty \\ &\leq \beta\left[w_b - \frac{2}{\pi}\,\mathrm{Si}\left(\frac{\pi w_b}{2}\right) + \mu\right] \triangleq \alpha.\end{aligned}$$

Therefore, the hypothesis of Theorem 4 are verified and hence Theorem 1 is proved. ■

B) Proof of Theorem 2:

Proof: Noticing that $\boldsymbol{\rho}(\mathbf{w}^*) = 0$, $\Delta\mathbf{w}^{(k)} = \mathbf{w}^{(k+1)} - \mathbf{w}^{(k)}$ and $\boldsymbol{\rho}(\mathbf{w}^{(k-1)}) = -D\boldsymbol{\rho}(\mathbf{w}^{(k-1)})\Delta\mathbf{w}^{(k-1)}$, a bound on the difference between the samples of the filtered PWM $\mathbf{y}^{(k)} = \mathbf{g}(\mathbf{w}^{(k)})$ that results of the use of the k-th iteration pulse width $\mathbf{w}^{(k)}$ and modulating signal samples $\mathbf{x} = \mathbf{g}(\mathbf{w}^*)$ can be computed as

$$\begin{aligned}&\|\mathbf{y}^{(k)} - \mathbf{x}\|_\infty \\ &= \|\mathbf{g}(\mathbf{w}^{(k)}) - \mathbf{g}(\mathbf{w}^*)\|_\infty \\ &= \|\boldsymbol{\rho}(\mathbf{w}^{(k)}) - \boldsymbol{\rho}(\mathbf{w}^*)\|_\infty \\ &= \|\boldsymbol{\rho}(\mathbf{w}^{(k)}) - \boldsymbol{\rho}(\mathbf{w}^{(k-1)}) + \boldsymbol{\rho}(\mathbf{w}^{(k-1)})\|_\infty \\ &= \|\boldsymbol{\rho}(\mathbf{w}^{(k)}) - \boldsymbol{\rho}(\mathbf{w}^{(k-1)}) - D\boldsymbol{\rho}(\mathbf{w}^{(k-1)})\Delta\mathbf{w}^{(k-1)}\|_\infty.\end{aligned}$$

From Lemma 3,

$$\begin{aligned}\|\mathbf{y}^{(k)} - \mathbf{x}\|_\infty &\leq \left(\frac{\gamma}{2}\right)\|\mathbf{w}^{(k)} - \mathbf{w}^{(k-1)}\|_\infty^2 \\ &\leq \left(\frac{\gamma}{2}\right)\|\mathbf{w}^{(k)} - \mathbf{w}^*\|_\infty^2.\end{aligned}$$

Finally, using Theorem 1,

$$\|\mathbf{y}^{(k)} - \mathbf{x}\|_\infty \leq \frac{\gamma\alpha^2}{2}\left(\frac{h^{2^k-1}}{1-h^{2^k}}\right)^2.$$

■

$$a_3(L,M)=\frac{[\psi^1(\underline{\ell}+1)+\psi^1\left(\overline{\ell}\right)]}{12}$$
$$a_5(L,M)=\frac{[-12\pi^2 a_3(L,M)+\psi^3(\underline{\ell}+1)+\psi^3\left(\overline{\ell}\right)]}{480}$$
$$a_7(L,M)=\frac{\{36\pi^4 a_3(L,M)-10\pi^2[\psi^3(\underline{\ell}+1)+\psi^3\left(\overline{\ell}\right)]+3[\psi^5(\underline{\ell}+1)+\psi^5\left(\overline{\ell}\right)]\}}{161280}$$

C) Proof of Theorem 3:

Proof: The worst case error occurs at instant $n=\underline{\ell}=(L-M)/2$. The $\underline{\ell}$-th sample of the filtered PWM (demodulated signal) is

$$y_{\underline{\ell}}=g_{\underline{\ell}}(\mathbf{w})=f_0\left(w_{\underline{\ell}}\right)+\sum_{k=1}^{\infty}f_k\left(w_{\underline{\ell}-k}\right)+f_k\left(w_{\underline{\ell}+k}\right)$$

and the value of this sample using block processing is

$$\breve{y}_{\underline{\ell}}=f_0\left(w_{\underline{\ell}}\right)+\sum_{k=1}^{L-1-\underline{\ell}}f_k\left(w_{\underline{\ell}+k}\right)+\sum_{k=1}^{\underline{\ell}}f_k\left(w_{\underline{\ell}-k}\right)$$

where $\breve{y}$ denotes the demodulated signal computed using only one block. The error at instant $\underline{\ell}=(L-M)/2$ is

$$e_B=y_{\underline{\ell}}-\breve{y}_{\underline{\ell}}=\sum_{k=L-\underline{\ell}}^{\infty}f_k(w_{\underline{\ell}+k})+\sum_{k=\underline{\ell}+1}^{\infty}f_k(w_{\underline{\ell}-k}). \quad (16)$$

The maximum error is achieved when the lateral areas of the sinc function add with the same sign to its maximum possible value. Under this assumption (16) can be written using μ and subtracting the contribution of area of the samples processed within the block, obtaining (10) in Theorem 3. To facilitate the computations, $\overline{e}_B$ may be approximated as

$$\overline{e}_B\approx a_3(L,M)w_b^3+a_5(L,M)w_b^5+a_7(L,M)w_b^7$$

replacing $f_m(w)$ in (16) with (17) (see Appendix B) for $m>0$. The coefficients a_i that depend on L and M are given by the equation at the top of the page, where $\psi^m(z)=(-1)^{m+1}m!\sum_{k=0}^{\infty}(z+k)^{-m-1}$ is the poly gamma function of order m. ■

Appendix B
Approximation of $f_m(w)$

The function $f_m(w)$ given by (5) depends on the integer variable $m\geq 0$ and on the real variable $|w|<1$. To avoid computation of the $\mathrm{Si}(.)$ function and the integral involved it can be approximated with a Taylor series as

$$f_m(w)=\begin{cases}b_0w+b_1w^3+b_2w^5+b_3w^7+R_7, & \text{if } m=0,\\ c_{1,m}w^3+c_{2,m}w^5+c_{3,m}w^7+R_7, & \text{if } m>0\end{cases} \quad (17)$$

where

$$b_0=1,$$
$$b_1=\frac{-\pi^2}{72},$$
$$b_2=\frac{\pi^4}{9600},$$
$$b_3=\frac{-\pi^6}{2257920},$$
$$c_{1,m}=\frac{-(-1)^m}{(12m^2)},$$
$$c_{2,m}=\frac{(-1)^m(112m^4\pi^2-672m^2)}{(53760m^6)},$$
$$c_{3,m}=\frac{(-1)^m(20m^2\pi^2-m^4\pi^4-120)}{(53760m^6)}.$$

Utilizing the mean value theorem the Lagrange reminder can be simplified to $R_7=w^8f_m^{(8)}(w^*)/8!$, where $f_m^{(8)}(w)$ is the 8th derivative of $f_m(w)$ with respect to w, and $w^*\in[0,w_b]$. Its maximum is obtained for $m=0$ and $w=w^*=1$ resulting in

$$\begin{aligned}R_7&\leq\frac{1}{8!}f_0^{(8)}(1)\\&=\frac{1}{\pi 8!}(-10080+1260\pi^2-\frac{105}{4}\pi^4+\frac{7}{32}\pi^6)\\&\approx 71.2\times10^{-6}.\end{aligned}$$

Evaluating $f_m(w)$ using (17) is fairly accurate and its computation is much simpler than using the $\mathrm{Si}(.)$ function.

This approximation can be used to compute the demodulated signal samples y_n. To make the computation of y_n causal, coefficients $c_{1,m}$, $c_{2,m}$ and $c_{3,m}$ are truncated to L samples, replacing (17) in (4), results in

$$y_n=\sum_{k=0}^{L-1}\left(h_{1,k}w_{n-k}+h_{3,k}w_{n-k}^3+h_{3,k}w_{n-k}^5+h_{3,k}w_{n-k}^7\right)$$

where for $k=0$: $h_{1,0}=b_0$, $h_{3,0}=b_1$, $h_{5,0}=b_2$, $h_{7,0}=b_3$ and for $k\neq 0$: $h_{1,k}=0$, $h_{3,k}=c_{1,k}$, $h_{5,k}=c_{2,k}$ and $h_{7,k}=c_{3,k}$.

Acknowledgment

The authors would like to thank the anonymous reviewers for their constructive comments.

References

[1] H. Black, *Modulation Theory*. New York: Van Nostrand, 1953.
[2] Z. Song and D. V. Sarwate, "The frequency spectrum of pulse width modulated signals," *Signal Process.*, vol. 83, no. 10, pp. 2227–2258, 2003.
[3] M. Margaliot and G. Weiss, "The low-frequency distortion in D-Class amplifiers," *IEEE Trans. Circuits Syst. II, Exp. Briefs*, vol. 57, no. 10, pp. 772–776, Oct. 2010.
[4] F. Chierchie and E. Paolini, "Quasi-analytical spectrum of PWM signals with dead-time for multiple sinusoidal input," in *Proc. IEEE Int. Symp. Circuits Syst. (ISCAS)*, Rio de Janeiro, Brazil, May 15–18, 2011, pp. 1033–1036.

[5] H. Mouton and B. Putzeys, "Understanding the PWM nonlinearity: Single-sided modulation," *IEEE Trans. Power Electron.*, vol. 27, no. 4, pp. 2116–2128, Apr. 2012.
[6] S. Caporale, R. Rovatti, and G. Setti, "Representation of PWM signals through time warping," in *Proc. IEEE Int. Conf. Acoust., Speech, Signal Process. (ICASSP)*, Mar. 2012, pp. 3589–3592.
[7] J. Fritzin, C. Svensson, and A. Alvandpour, "Design and analysis of a Class-D stage with harmonic suppression," *IEEE Trans. Circuits Syst. I, Reg. Papers*, vol. 59, no. 6, pp. 1178–1186, Jun. 2012.
[8] G. Smecher and B. Champagne, "Optimum crossing-point estimation of a sampled analog signal with a periodic carrier," *Signal Process.*, vol. 91, no. 8, pp. 1951–1962, 2011.
[9] E. Alarcon, D. Fernandez, A. Garcia i Tormo, J. Madrenas, and A. Poveda, "Continuous-time CMOS adaptive asynchronous $\Sigma\Delta$ modulator approximating low-f_s low-inband-error on-chip wideband power amplifier," *Proc. IEEE Int. Symp. Circuits Syst. (ISCAS)*, pp. 301–304, May 2011.
[10] J. Yu, M. T. Tan, W. L. Goh, and S. Cox, "A dual-feedforward carrier-modulated second-order Class-D amplifier with improved THD," *IEEE Trans. Circuits Syst. II, Exp. Briefs*, vol. 59, no. 1, pp. 35–39, Jan. 2012.
[11] A. Lazar and L. Toth, "Perfect recovery and sensitivity analysis of time encoded bandlimited signals," *IEEE Trans. Circuits Syst. I, Reg. Papers*, vol. 51, no. 10, pp. 2060–2073, Oct. 2004.
[12] A. Lazar, E. Simonyi, and L. Toth, "An overcomplete stitching algorithm for time decoding machines," *IEEE Trans. Circuits Syst. I, Reg. Papers*, vol. 55, no. 9, pp. 2619–2630, Oct. 2008.
[13] B. Logan, Jr, "Click modulation," *AT&T Bell Labs. Tech. J.*, vol. 63, no. 3, pp. 401–423, 1984.
[14] L. Stefanazzi, E. Paolini, and A. Oliva, "Click modulation: An off-line implementation," in *Proc. Midwest Symp. Circuits Syst. (MWSCAS)*, Knoxville, TN, USA, Aug. 10–13, 2008, pp. 946–949.
[15] M. Streitenberger, H. Bresch, and L. Mathis, "Theory and implementation of a new type of digital power amplifier for audio applications," in *Proc. IEEE Int. Symp. Circuits Syst. (ISCAS)*, Geneva, Switzerland, 2000, vol. 1, pp. 511–514.
[16] L. Stefanazzi, A. Oliva, and E. Paolini, "Alias-free digital click modulator," *IEEE Trans. Ind. Inf.*, vol. 9, no. 2, pp. 1074–1083, May 2013.
[17] A. Garcia i Tormo, A. Poveda, E. Alarcon, and F. Guinjoan-Gispert, "Fundamental modulation limits for minimum switching frequency in-band-error-free high-efficiency power amplifiers," *IEEE Trans. Circuits Syst. I, Reg. Papers*, vol. 58, no. 10, pp. 2543–2555, Oct. 2011.
[18] J. Huang, K. Padmanabhan, and O. Collins, "The sampling theorem with constant amplitude variable width pulses," *IEEE Trans. Circuits Syst. I, Reg. Papers*, vol. 58, no. 6, pp. 1178–1190, Jun. 2011.
[19] S. O. Aase, "A prefilter equalizer for pulse width modulation," *Signal Process.*, vol. 92, no. 10, pp. 2444–2453, 2012.
[20] Texas Instruments, "High-resolution pulse width modulator (HRPWM)," Lit. No. SPRU924F. Dallas, TX, USA, 2011 [Online]. Available: http://www.ti.com/lit/ug/spru924f/spru924f.pdf
[21] A. de Castro and E. Todorovich, "High resolution FPGA DPWM based on variable clock phase shifting," *IEEE Trans. Power Electron.*, vol. 25, no. 5, pp. 1115–1119, 2010.
[22] D. Navarro, O. Lucía, L. A. Barragán, J. I. Artigas, I. Urriza, and O. Jiménez, "Synchronous FPGA-based high-resolution implementations of digital pulse-width modulators," *IEEE Trans. Power Electron.*, vol. 27, no. 5, pp. 2515–2525, May 2012.
[23] P. Diniz, E. Da Silva, and S. Netto, *Digital Signal Processing: System Analysis and Design*. Cambridge, U.K.: Cambridge Univ. Press, 2010.
[24] H. Liu and Q. Ni, "Incomplete Jacobian Newton method for nonlinear equations," *Comput. Math. With Appl.*, vol. 56, no. 1, pp. 218–227, 2008.
[25] J. Stoer and R. Bulirsch, *Introduction to Numerical Analysis*. New York: Springer-Verlag, 1992.
[26] M. Waziri, W. Leong, M. Hassan, and M. Monsi, "Jacobian computation-free Newton method for systems of non-linear equations," *J. Numerical Math. Stochastic*, vol. 2, no. 1, pp. 54–63, 2010.
[27] A. V. Oppenheim and R. Schafer, *Discrete-Time Signal Processing*. Englewood Cliffs, NJ, USA: Prentice-Hall, 1989.

Fernando Chierchie (GS'10) received his B.S. degree in electronic engineering in 2009 and his M.S. degree in control systems in 2011 both from Universidad Nacional del Sur, Bahía Blanca, Argentina. He is a Teaching Assistant at at Universidad Nacional del Sur. His research interests are switching amplifiers, signal processing, power electronics, and DSP implementations of digital control and signal processing algorithms. He is a member of the IEEE Circuits and Systems Society.

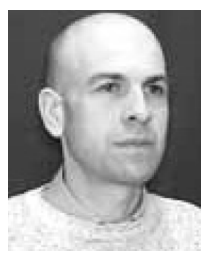

Eduardo E. Paolini is Adjunct Professor at Universidad Nacional del Sur, Bahía Blanca, Argentina, since 1998, and a member of Comisión de Investigaciones Científicas de la Provincia de Buenos Aires (CIC) since 2011. His research interests are digital signal processing, and switched and nonlinear systems.